

# RSC Advances



This is an *Accepted Manuscript*, which has been through the Royal Society of Chemistry peer review process and has been accepted for publication.

*Accepted Manuscripts* are published online shortly after acceptance, before technical editing, formatting and proof reading. Using this free service, authors can make their results available to the community, in citable form, before we publish the edited article. This *Accepted Manuscript* will be replaced by the edited, formatted and paginated article as soon as this is available.

You can find more information about *Accepted Manuscripts* in the [Information for Authors](#).

Please note that technical editing may introduce minor changes to the text and/or graphics, which may alter content. The journal's standard [Terms & Conditions](#) and the [Ethical guidelines](#) still apply. In no event shall the Royal Society of Chemistry be held responsible for any errors or omissions in this *Accepted Manuscript* or any consequences arising from the use of any information it contains.

**Mechanism of cytotoxicity of micron/nano calcium oxalate monohydrate  
and dihydrate crystals on renal epithelial cells**

Xin-Yuan Sun, Jian-Ming Ouyang\*, Yu-Bao Li, Xiao-Ling Wen

(Department of Chemistry, Jinan University, Guangzhou 510632, China; Institute of  
Biomineralization and Lithiasis Research, Jinan University, Guangzhou 510632, China)

---

Corresponding authors. *E-mail address:* [toyjm@jnu.edu.cn](mailto:toyjm@jnu.edu.cn)

**Abstract:** Urinary crystals in normal and kidney stone patients often contain a larger proportion of micron/nano calcium oxalate monohydrate (COM) and calcium oxalate dihydrate (COD) crystals. However, the difference of their varying sizes and crystal phases in inducing the formation of kidney stone remains unclear. This study aims to investigate comparatively the cytotoxicity and aggregation capabilities of micron/nano COM and COD *in vitro* to reveal the mechanism of kidney stone formation. The effect of the exposure 50 nm (COM-50nm and COD-50nm) and 10  $\mu\text{m}$  (COM-10 $\mu\text{m}$  and COD-10 $\mu\text{m}$ ) calcium oxalate crystals toward the African green monkey renal epithelial (Vero) cells were investigated by detecting cell viability, cell membrane integrity, cell morphology change, adhesion and internalization, intracellular reactive oxygen species (ROS), mitochondrial membrane potential ( $\Delta\psi\text{m}$ ), cell cycle progression, and cell death rate by apoptosis and/or necrosis. The cell viability and cytomembrane integrity of Vero cells were significantly decreased in size- and concentration-dependent manners after the treatment of micron/nano COM and COD crystals. Cell injury increased with the reduction in crystal size and increase in crystal concentration; COM caused a more serious injury in Vero than COD with the same size. COM-10 $\mu\text{m}$  and COD-10 $\mu\text{m}$  caused mild injury in Vero because they could only adhere on the cell surface and could not be completely internalized into cells. Meanwhile, the adhered COM-50nm and COD-50nm were further internalized into cells, caused severe injury, and the effects were more concentration-dependent. Excessive expression of ROS further led to the decrease of  $\Delta\psi\text{m}$  and cell cycle dysregulation; a series of cell response ultimately caused significant number of necrotic cell deaths and few apoptotic cell deaths. Micron-sized COM and COD crystals induced cell injury by damaging the membrane integrity. Nano-COM and COD crystals could damage membrane integrity by adhering crystals, as well as directly damage the mitochondria by internalized crystals. Thus, Nano-sized crystals possess greater toxicity than micron-sized crystals.

**Keywords:** Micron/nano calcium oxalate crystals; Size-dependent toxicity; Internalization, Cell injury

## 1. Introduction

Calcium oxalate (CaOx) is the major crystalline component in kidney stones, including two main hydrates, namely, calcium oxalate monohydrate (COM) and calcium oxalate dihydrate (COD) [1,2]. Most stones contain COM as the major component, while COD is significantly less prevalent [3].

Crystal-cell interactions, including crystal attachment and endocytosis, are important processes in the formation of CaOx stone [4,5]. Kohjimoto et al. [6] indicated that crystal-cell interactions may be among the earliest processes in the formation of kidney stones. Khan et al. [7] also concluded that crystal attachment and endocytosis are essential factors in inducing cell injury and follow the formation of urinary stone. For papillary COM stone formation, the attachment of crystals to the damaged renal tubular epithelial cell is necessary for the initiation of stone formation [8].

The exposure of COM crystals could activate reactive oxygen species (ROS) production, which originated from the mitochondria in renal epithelial cells, thereby leading to mitochondrial damage [5]. Mitochondria are significant sources of ROS produced in renal cells [9]. Meimaridou et al. [10] demonstrated that mitochondrial  $O_2^{\cdot-}$  in COM treated cells was enhanced by three to fourfold compared with the controls. The intracellular dissociation of COM and the mitochondrial dicarboxylate transporter are important in  $O_2^{\cdot-}$  production. Recent evidence also suggests that COM crystals could cause the changes in gene expression and significantly alter the global expression profile of miRNAs *in vitro* [11].

Compared with the extensive number of research on the injury effect of COM crystals, cell injury induced by COD crystals remains rare [12-14]. Semangoen et al. [12] indicated that the percentage of cell death do not significantly differ between cells with and without COD crystal adhesion. However, COD exposure could alter the protein expression, including metabolic enzymes,

cellular structural protein, calcium-binding protein, adhesion molecule, protein involved in RNA metabolism, and chaperone. Yuen et al. [13] also found that HK-2 cells displayed mild cellular damage within 18 h post COD exposure; however, prolonged incubation caused significant damage to disrupt the monolayer integrity and increase the released hyaluronan disaccharides in the harvested media. The cytotoxicity of COD crystals toward African green monkey renal epithelial (Vero) cells was found to be size-dependent and increases in the order 50 nm > 100 nm > 600 nm > 3  $\mu\text{m}$  > 10  $\mu\text{m}$  [14].

The formation of stones appears to depend on the crystalline form of CaOx in urine. COM was more likely to adhere on the surface of cells than COD [15]. About 50% more COM than COD appears to bind to the IMCD cells for a given amount of added crystals [16]. Studies have shown that the content of COM in calculi patients is higher than in the healthy controls, whereas the content of COD is lower [4].

The urine of normal persons and kidney stone patients often have varying sizes of COM and COD crystals [17,18]; however, the injury difference of CaOx crystals with different sizes and crystal phases toward renal tubular epithelial cells remains unclear. Moreover, the differences in cell injury caused by micron/nano COM and COD in urine have not been reported yet.

We studied the differences in the injury ability of nano-sized (about 50 nm) and micron-sized (about 10  $\mu\text{m}$ ) COM and COD crystals in Vero cells comparatively to elaborate the mechanism of cell injury caused by the varying sizes and crystal phases of CaOx crystals at cellular and molecular levels and provide new insights into the inhibition of kidney stone formation in clinical settings

## **2. Materials and methods**

### **2.1 Materials and apparatus**

(1) Materials: African green monkey renal epithelial (Vero) cells were purchased from Shanghai

Cell Bank, Chinese Academy of Sciences (Shanghai, China). DMEM culture medium was purchased from HyClone Biochemical Products Co., Ltd. (UT, USA). Fetal bovine serum was purchased from Hangzhou Sijiqing Biological Engineering Materials Co., Ltd. (Hangzhou, China). Penicillin and streptomycin were purchased from Beijing Pubo Biotechnology Co., Ltd. (Beijing, China). Cell culture plates were purchased from Wuxi Nest Bio-Tech Co., Ltd. (Wuxi, China).

Cell proliferation assay kit (CCK-8) was purchased from Dojindo Laboratories (Kumamoto, Japan). Lactate dehydrogenase (LDH) kit was purchased from Shanghai Beyotime Bio-Tech Co., Ltd. (Shanghai, China). Annexin V-FITC, 5,5',6,6'-Tetrachloro-1,1',3,3'-tetraethylimidacarbocyanine iodide (JC-1), propidium iodide (PI) and 2',7'-dichlorodihydrofluorescein diacetate (DCFH-DA) were all purchased from Becton, Dickinson and Company in USA. All conventional reagents used were analytically pure and purchased from Guangzhou Chemical Reagent Factory of China (Guangzhou, China).

(2) Apparatus: The apparatus used include X-L type environmental scanning electron microscope (SEM, Philips, Eindhoven, Netherlands), laser confocal microscope (LSM510 Meta Duo Scan, Zeiss, Jena, Germany), enzyme mark instrument (Safire2™, Tecan, Männedorf, Switzerland), flow cytometer (FACS Aria, BD Corporation, CA, USA). Nano-ZS nanoparticle size and zeta potential analyzer (Malvem, UK), D/max2400X X-ray powder diffractometer (Rigaku). Tristar 3000 surface area and porosity analyzer (Micromeritics, American).

## 2.2 Experimental methods

### 2.2.1 Preparation of COM and COD crystals and crystal suspensions

Four kinds of COM and COD crystals (COM-50nm, COM-10μm, COD-50nm and COD-10μm) were prepared by changing the concentration of reactants (CaCl<sub>2</sub> and Na<sub>2</sub>Ox), reaction

temperature, solvent and stirring speed. For COM-50nm, 100 mmol/L  $\text{CaCl}_2$  and  $\text{K}_2\text{Ox}$  solution were each prepared in anhydrous ethanol–water mixture solution ( $V_{\text{H}_2\text{O}}: V_{\text{ethanol}} = 1: 1$ ). Then, 50 mL of each solution was rapidly mixed under high stirring speed (1250 rpm) for 6 min at 25°C. For COM-10 $\mu\text{m}$ , 50 mL of 40 mmol/L  $\text{CaCl}_2$  was added to 300 mL of double-distilled water in a thermostat water bath at 75°C, and then 50 mL of 40 mmol/L  $\text{K}_2\text{Ox}$  was added dropwise to the above solution at the speed of 0.5 drops/s for 45 min. The reaction solution was stirred at 250 rpm for 2 min after complete addition, and incubated overnight at room temperature. For COD-50nm, 12 mL  $\text{CaCl}_2$  solution (4 mol/L) was added into 200 mL buffer solution (pH=6.8) at 5°C, and then directly poured 50 mL  $\text{K}_2\text{Ox}$  solution (250 mmol/L) at 1250 rpm stirring for 5 min. For COD-10 $\mu\text{m}$ , 1.56 mL  $\text{CaCl}_2$  solution (4 mol/L) was added into 500 mL buffer solution, and then 12.8 mL  $\text{K}_2\text{Ox}$  solution (0.25 mol/L) was slowly added into the above solution at the speed of 2 drops/s under low speed stirring (200 rpm) at 25°C. The reaction solution was further stirred for 2 min after complete addition, and incubated overnight at room temperature. All the prepared samples were washed twice with anhydrous ethanol under ultrasound treatment, and then the crystals were collected by suction filtration and dried in drying oven for 24 h.

The morphology, size and crystalline phase of prepared crystals were characterized by SEM and XRD. Image Pro Plus 5.02 (Media Cybernetics, USA) was used to analyze the size and count the number of crystals. The hydrodynamic sizes and zeta potential of COM and COD crystals in DMEM culture media were measured by nanoparticle size and zeta potential analyzer. Sizes are expressed as Z-average values. The surface area of  $\text{CaOx}$  was measured by Tristar 3000 surface area and porosity analyzer.

For the preparation of micron/nano COM and COD crystal suspensions, a certain amount of COM or COD crystals were UV sterilized for 40 min and dispersed in serum-free DMEM culture

medium to form crystal suspensions with the concentration of 100, 300 and 1000  $\mu\text{g/mL}$ , respectively.

### 2.2.2 Cell culture

Vero cells were cultured in DMEM culture medium containing 10% fetal bovine serum in a 5%  $\text{CO}_2$  humidified atmosphere at  $37^\circ\text{C}$ . Trypsin digestion method was adopted for cell propagation. Upon reaching 80%–90% confluence, the cells were rinsed twice with PBS. A certain amount of 0.25% trypsin digestion solution was then added and maintained for 3–5 min at  $37^\circ\text{C}$ . Afterward, DMEM containing 10% fetal bovine serum was added to terminate digestion. The cells were then blown gently to form cell suspension for the following cell experiment.

### 2.2.3 Cell viability assay

One hundred microliters of cell suspension with a cell concentration of  $1 \times 10^5$  cells/mL was inoculated per well in 96-well plates and incubated for 24 h. Afterward, the medium was changed to serum-free culture media and then incubated for another 12 h to achieve synchronization. The culture medium was removed by suction and the cells were washed twice with PBS. The experimental model was divided into two groups: (A) control group, in which only serum-free culture medium was added; (B) treatment group with COM or COD crystals, in which cells were exposed to 50 nm, 10  $\mu\text{m}$  COM and COD with the concentration of 100, 300 and 1000  $\mu\text{g/mL}$  prepared with serum-free culture medium, respectively. Each experiment was repeated in three parallel wells. After incubation for 6 h, 10  $\mu\text{l}$  CCK-8 was added to each well and incubated for 1.5 h. Absorbance (A) was measured by using the enzyme mark instrument at 450 nm. Cell viability was determined using the equation below.

$$\text{Cell viability (\%)} = \frac{A(\text{treatment group})}{A(\text{control group})} \times 100$$

### 2.2.4 Lactate dehydrogenase (LDH) release assay

One hundred microliters of cell suspension with a cell concentration of  $1 \times 10^5$  cell/mL was inoculated per well and incubated for 24 h. Afterward, the medium was changed to serum-free culture media and then incubated for another 12 h to achieve synchronization. The experimental model was divided into four groups: (A) cell-free culture medium wells (control wells of background); (B) control wells without drug treatment (sample control wells); (C) cells without drug treatment for the subsequent cleavage of the wells (sample maximum enzyme activity control wells); and (D) treated group with 50 nm, 10  $\mu$ m COM and COD at the concentration of 100, 300 and 1000  $\mu$ g/mL (drug-treated wells). After incubation, the absorbance was analyzed at 490 nm according to the LDH kit instruction.

$$\text{LDH\%} = \frac{A(\text{Group D}) - A(\text{Group A})}{A(\text{Group C}) - A(\text{Group A})} \times 100$$

### 2.2.5 Scanning electron microscope observation

The density of seeded cells and experimental grouping were the same as those detected by LDH release assay. After reaching the adhesion time, the supernatant was removed by suction, washed three times with PBS, fixed in 2.5% glutaraldehyde at 4°C for 24 h, and then fixed with 1% OsO<sub>4</sub>, washed three times with PBS, dehydrated in gradient ethanol (30%, 50%, 70%, 90% and 100%, respectively), dried under the critical point of CO<sub>2</sub>, and treated with gold sputtering. Vero cells treated by COD and COM crystals were observed by SEM.

### 2.2.6 Confocal microscopy observation

A combination of light reflection (to visualize the crystals) and fluorescent-labeled phalloidin and 4',6-diamidino-2-phenylindole (DAPI) (to visualize the cells) was used to monitor the fate of cell-associated crystals by confocal microscopy. Approximately 1 mL of cell suspension with a cell concentration of  $1 \times 10^5$  cells/mL was inoculated per well in 12-well plates for 12 h. The 50 nm and 10  $\mu$ m nonradiolabeled COM crystals with a concentration of 200  $\mu$ g/mL were incubated with

subconfluent cultures at 37°C. After 6 h of incubation, the supernatant was aspirated and the cells were washed twice with PBS. All nonattached crystals were removed by extensive washings. Afterward, the cells were fixed for 30 min with paraformaldehyde (4%) in PBS, followed by three times membrane permeabilization with 0.1% Triton X-100 in PBS at room temperature for 5 min. The inserts were incubated for 60 min with 200 µL fluorescein isothiocyanate (FITC)-conjugated phalloidin and then washed twice with 0.1% Triton X-100. DAPI staining solution was then added to the cells and incubated for 5 min. The cells were again washed three times with PBS for 5 min. Finally, the prepared samples were mounted with anti-fade fluorescence mounting medium and observed in a confocal microscope. A 488 nm and a 405 nm argon lasers were used to excite the FITC-phalloidin and the DAPI nuclear dyes, respectively. The extracellularly adhered crystals and intracellularly internalized crystals were visualized by their ability to reflect the light at  $\lambda$  633 nm of Kr-laser in red.

### 2.2.7 Intracellular ROS assay

Two milliliters of cell suspension with a cell concentration of  $1 \times 10^5$  cells/mL was inoculated per well in six-well plates. After synchronization, the cells were grouped. 300 µg/mL micron/nano COD and COM crystals were then added. After 6 h incubation, the supernatant was aspirated and the cells were washed twice with PBS and digested with 0.25% trypsin. Afterward, DMEM supplemented with 10% fetal bovine serum was added to terminate digestion. The cells were suspended by pipetting, followed by centrifugation (1000 rpm, 5 min). The supernatant was aspirated and the cells were washed once with PBS and centrifuged again to obtain a cell pellet. The cells were resuspended by adding and thoroughly mixing 500 µl PBS in a microcentrifuge tube. The samples were then stained with 2', 7'-dichloro-fluorescein diacetate (DCFH-DA) and analyzed.

### 2.2.8 Measurement of mitochondrial membrane potential ( $\Delta\psi_m$ )

The density of seeded cells and experimental grouping were the same as ROS assay. After 6 h of incubation with micron/nano COD and COM crystals at the concentration of 100, 300 and 1000  $\mu\text{g/mL}$ , the supernatant was aspirated and the cells were washed twice with PBS and digested with 0.25% trypsin. DMEM supplemented with 10% fetal bovine serum was then added to terminate digestion. The cells were suspended by pipetting, followed by centrifugation (1000 rpm, 5 min). The supernatant was aspirated and the cells were washed with PBS and centrifuged again to obtain a cell pellet. The cells were resuspended by adding and thoroughly mixing 500  $\mu\text{L}$  of PBS in a microcentrifuge tube. Finally, the samples were stained with JC-1 and then analyzed.

### **2.2.9 Cell cycle progression assay**

Two milliliter of cell suspension with a cell concentration of  $1.5 \times 10^5$  cells/mL was inoculated per well in 6-well plates for 24 h. After synchronization, incubated with 300  $\mu\text{g/mL}$  micron/nano COD and COM crystals for 6 h, the collected cells were washed twice with PBS and centrifugation (1000 rpm, 5 min), then fixed using 70% ethanol for 12 h at  $4^\circ\text{C}$ . Ethanol was removed by centrifugation (2000 rpm, 5 min), and the cells were washed twice with PBS. Cells were then resuspended in 200  $\mu\text{L}$  propidium iodide and kept at  $37^\circ\text{C}$  for 15 min. The cell cycle was analyzed by measuring the amount of PI-labeled DNA in fixed cells by the flow cytometer.

### **2.2.10 Cell death assay**

Apoptosis and necrosis induced by micron/nano COD and COM crystals in Vero cells was measured by FCM with Annexin V-FITC/PI double staining assay. Briefly, the cells were harvested after 6 h of exposure to micron/nano COD and COM crystals at the concentration of 100, 300 and 1000  $\mu\text{g/mL}$ , and then stained using Annexin V-FITC/PI cell death assay kit according to the manufacturer's instructions. About  $1.5 \times 10^5$  cells were collected and washed with PBS (centrifuged at 1000 rpm for 5 min). The cells were resuspended in 200  $\mu\text{L}$  binding buffer. Afterward, 5  $\mu\text{L}$

Annexin V–FITC was added and then incubated in darkness at room temperature for 10 min. The cells were again resuspended in 200  $\mu$ L binding buffer and stained with 5  $\mu$ L PI. The prepared cells were then analyzed using a flow cytometer.

### 3 Results

#### 3.1 Characterization of micron/nano COM and COD crystals

COM and COD crystals of varying sizes (50 nm and 10  $\mu$ m) were prepared by changing the concentrations of reactant ( $\text{Na}_2\text{Ox}$  and  $\text{CaCl}_2$ ), reaction temperature, solvent and stirring speed. The morphology, crystal size and crystal phase were detected by SEM and XRD characterization, all prepared crystals were the target products (Fig.1). COM–50nm and COD–50nm was mainly of spheroid, COM–10 $\mu$ m mainly presented the most common morphology of hexagonal lozenge, and COD–10 $\mu$ m was mainly of tetragonal bipyramid. By measuring the diameters of 100 crystals directly from the SEM images, the size distributions of the four micron/nano COM and COD crystals are presented in Table 1. Since the average size of four crystals was nearly 50 nm and 10  $\mu$ m respectively, we used an integer to represent crystal size for convenient. That is, COM-50nm, COM-10 $\mu$ m, COD-50nm, and COD-10 $\mu$ m were used to represent these four different-sized crystals, respectively. COM–50nm and COD–50nm was mainly of spheroid, COM–10 $\mu$ m mainly presented the most common morphology of hexagonal lozenge, and COD–10 $\mu$ m was mainly of tetragonal bipyramid.

Table 1 also shows the detected specific surface area  $S_{BET}$ , zeta potentials, and hydrodynamic sizes in DMEM. Compared with micron-sized  $\text{CaOx}$ , the COM-50nm and COD-50nm were aggregated more easily in the culture medium because of their low zeta potential and larger specific surface area. The detected hydrodynamic sizes of COM-50nm and COD-50nm ( $1342 \pm 131$  nm and  $953 \pm 98$  nm, respectively) were also much larger than the sizes of SEM characterization ( $47.7 \pm 6.2$  nm and  $44.1 \pm 8.7$  nm, respectively); however, COM-10 $\mu$ m and COD-10 $\mu$ m displayed good dispersion and stability (Fig. 1).

### 3.2 Effects of COM and COD crystals exposure on cellular viability of Vero cells

CCK-8 assay estimates the number of living cells depending on the integrity of mitochondrial function. The viability of Vero cells was detected by CCK-8 assay after 6 h exposure to different concentrations (100, 300, and 1000  $\mu\text{g}/\text{mL}$ ) of micron/nano COM and COD crystals (Fig. 2a). The four crystals presented concentration-dependent toxicity in Vero cells; cell viability decreased with the increase in crystal concentration. Two nano crystals of COM-50nm and COD-50nm caused the cell viability to decrease more obviously than the two micron-sized crystals of COM-10 $\mu\text{m}$  and COD-10 $\mu\text{m}$ . Furthermore, COM showed higher toxicity than COD under the same size and crystal concentration.

### 3.3 Cytomembrane damage of Vero cells induced by COM and COD crystals

LDH is a stable enzyme of the cytoplasm that is released extracellularly once the cell membrane ruptures. Thus, LDH is considered as a marker of cell membrane integrity. The amount of released LDH caused by COM-50nm was much higher than COD-50nm under the same concentration (Fig. 2b), indicating that nano COM caused cell membrane ruptures much easier than the nano COD. Compared with the control group, COM-10 $\mu\text{m}$  and COD-10 $\mu\text{m}$  could also increase LDH release; COM-10 $\mu\text{m}$  caused more LDH release than COD-10 $\mu\text{m}$  under low concentration.

### 3.4 Cell and crystal morphology observation by SEM

For the visual detection of the potential toxicity of CaOx in Vero cells, the morphology variation of Vero cells was detected by SEM after exposure to 300  $\mu\text{g}/\text{mL}$  micron/nano COM and COD crystals for 6 h (Fig. 3). The treated cells of the COM-50nm and COD-50nm groups distorted with much abnormal morphology, the microvillus ruptured, and a large number of crystals aggregated on cell surface. Compared with the nano-sized crystal treated groups, only a small number of crystals adhered to the cells treated by COM-10 $\mu\text{m}$  and COD-10 $\mu\text{m}$ ; the adhered crystals caused cell membrane sunk and even fractured.

The exposed crystals, specifically COD-10 $\mu$ m, in the cell culture medium were observed for obvious corrosion phenomenon, which may be related to the cell membrane being ruptured after cell injury. Several hydrolytic enzymes in lysosomes, such as proteases, lipases, nucleases, glycosidases, phospholipases, phosphatases, and sulfatases [19] were released extracellularly and caused crystal corrosion.

### 3.5 Confocal microscopy observation of crystal distribution in Vero cells

COM crystals could be visualized by their ability to reflect the light at  $\lambda$  633 nm of Kr-laser in red [20]; however, COD crystals do not possess such property. Therefore, to assess the fate of cell surface-associated crystals with the size of 50 nm and 10  $\mu$ m, we selected nonradiolabeled and non-fluorescentlabeled COM-50nm and COM-10 $\mu$ m to assess the distribution of varying crystal sizes in Vero cells.

Fig. 4 shows the two-dimensional confocal images perpendicular to the surface of the cells. Results confirmed that plain COM crystals could be visualized in red at  $\lambda$  633 nm (Fig. 4A). Cells presented smooth plump morphology and mainly showed spindle forms in the control group (Fig. 4B). The cytoskeleton appeared disorganized and nucleus fragmentations were observed in the COM-50nm treated groups. COM-50nm could adhere on the cell surface (indicated by the arrowhead in Fig. 4C), as well as pass through the cell membrane and be internalized into cells (indicated by the open arrow in Fig. 4C), Internalized COM crystals are distributed in the cytoplasm and even could directly interact with the cell nucleus. COM-10 $\mu$ m was only observed on the cell surface (indicated by the arrowhead in Fig. 4D) or partly be embedded in the cell membrane whereas the cytoskeleton appeared to be severely disorganized in the cells with adhesive crystals.

### 3.6 Intracellular ROS generation induced by COM and COD crystals

Mitochondria are generally the most common source of superoxide and hydrogen peroxide in most cells and tissues. Membrane-associated nicotinamide adenine dinucleotide phosphate (NADPH) oxidase is also a major source of ROS in the kidneys. When ROS formation overwhelms endogenous and/or exogenous antioxidant capacity, the cellular redox balance becomes altered and oxidative stress ensues.

The intracellular ROS level was determined to further elucidate the mechanisms of cytotoxicity induced by micron/nano COM and COD crystals (Fig. 5A). The generated ROS in the four crystal-treated groups increased compared with the control group. However, the nano-sized crystal-treated groups caused more significant increase in ROS than the micron-sized crystal treated groups (Fig. 5B). The ROS increase induced by COM was higher than COD with the same size, specifically in the micron-sized treated groups.

### 3.7 Decrease in $\Delta\psi_m$ caused by COM and COD crystals

Apoptosis and necrosis are often preceded by mitochondrial dysfunction, in particular, a loss of mitochondrial membrane potential ( $\Delta\psi_m$ ). Mitochondria have high  $\Delta\psi_m$  potential under normal circumstances, and would become depolarized after suffering injury. Calculating the changes in the ratio (R/G) of emitted red fluorescence at 596 nm (high  $\Delta\psi_m$ ) and green fluorescence at 534 nm (low  $\Delta\psi_m$ ) provides a qualitative estimate of the changes in  $\Delta\psi_m$ .

The JC-1 dye was used to determine the effects of the different concentrations of micron/nano COM and COD exposure on the ( $\Delta\psi_m$ ) in Vero (Fig.6). The R/G ratios decreased in size- and concentration-dependent manners. The four crystals could cause a continuous decline of  $\Delta\psi_m$  with the increase in crystal concentration from 100  $\mu\text{g/mL}$  to 1000  $\mu\text{g/mL}$ , wherein the nano crystal caused more significant decrease in  $\Delta\psi_m$  than the micron-sized crystals. Meanwhile, the decrease in  $\Delta\psi_m$  caused by COM was slightly higher than COD with the same size. Nano-sized crystals caused more significant  $\Delta\psi_m$  decrease than the micron-sized crystals at low concentration, whereas all

crystals caused the largest decline in  $\Delta\psi_m$ , with similar R/G ratios at high concentration.

The decrease in  $\Delta\psi_m$  was consistent with the varying patterns of cell viability and LDH release (Fig. 2). The capacity of disrupting the mitochondrial function was ranked in the following order: COM-50nm > COD-50nm >> COM-10 $\mu$ m > COD-10 $\mu$ m.

### 3.8 Cell cycle arrest of Vero cells caused by COM and COD crystals

The Vero cell cycle was evaluated to continue the investigation on the toxicity of micron/nano COM and COD. Fig. 7 shows the representative experiment results of the propidium iodide (PI) fluorescence intensity, which was proportional to the DNA content and indicated the cell cycle phases.

Compared with the control group (69.33% G1 phase and 19.67% S phase), the COD-50nm and COM-50nm treatment of Vero at 300  $\mu$ g/ml significantly caused the cells with DNA content to decrease in the G1 phase (58.87% and 61.10%, respectively) and increase in the S phase (31.58% and 32.70%, respectively) of the cell cycle. These results indicated that the cell cycle was arrested at the S phase. Moreover, the cell number in the S phase of the COM-50nm treated group was slightly higher than in COD-50nm treated group. The COM-10 $\mu$ m and COD-10 $\mu$ m treated groups did not show any obvious change in the G1, S, and G2 phases. The cells of nano-sized COM and COD treatment groups in the S phase increased significantly than in the micron-sized crystals treatment group, which may cause easier penetration of the nano crystals to the cell membrane than the micron-sized crystals. The internalized crystals could directly interact with the nucleus, and even the DNA in the nucleus, thereby causing the S phase arrest.

### 3.9 Cell death induced by COM and COD crystals

To assess the nature of crystal-induced cell death, we performed flow cytometric analysis to quantify the apoptotic and necrotic cells using annexin V/PI double staining (Fig. 8). Annexin V staining was applied to reveal the surface exposure of phosphatidylserine (apoptosis), while PI was

applied to reveal the loss of plasma membrane integrity (necrosis).

The cell death rate ( $Q1+Q2+Q4$ ) in the COM-50nm and COD-50nm treated groups was higher than in the COD-10 $\mu$ m and COM-10 $\mu$ m treated groups; all death rates increased with the increase in crystal concentration. Under the same crystal concentration, COM-50nm caused much higher death rate than COD-50nm. The number of necrotic cells (Quadrant Q1) in the nano-sized COM and COD treated groups was also much higher than in the micron-sized COM and COD treated groups; the necrosis rate accounted for the largest proportion in the total mortality. Quadrant Q2 shows the cells stained with both Annexin V and PI, which presented the number of necrotic and/or late apoptotic cells; it was also the same concentration-dependent. The number of early apoptosis cells (Q4) in the four treated groups had no obvious change compared with the control group; only a small amount of increase occurred at high concentrations.

#### 4. Discussion

The cytotoxicity of micron/nano CaOx was ranked in the following order: COM-50nm > COD-50nm >> COM-10 $\mu$ m > COD-10 $\mu$ m. The injury mechanism in Vero cells induced by micron/nano COM and COD crystals was significantly different as a result of crystal size, crystal phase, and their distribution in cells.

##### 4.1 Micron-sized COM and COD produce toxicity by damaging the cell membrane integrity

The cells had difficulty in completely internalizing COM-10 $\mu$ m and COD-10 $\mu$ m because of their large sizes, thus they could only adhere on the cell surface or be partly internalized (Fig. 4). The toxicity mechanism of micron-sized COM and COD induced cell death, which could be summarized in the schematic illustration in Fig. 9. Meanwhile, the adhered micron-sized crystals on the cell membrane could directly interact with the subcellular structure, leading to cell membrane damage, cell permeability change, and even membrane fracture (Fig. 3), thereby causing cell necrosis.

Moreover, the adhered crystals on the cell membrane could activate cyclophilin D, cause mitochondrial collapse, and produce oxidative stress (Fig. 4), which consequently causes cell injury

and even cell death [21]. The region of the cell membrane where the crystals adhered becomes fragile or even fractured (Figs. 3c and 3d). The cell membrane in the fractured cells lack protection, hence the cytoplasm flowed out and the intracellular environment is destroyed, thereby leading to cell death. After COM and COD adhered to the Vero cell membrane, the LDH levels increased (Fig. 2b), which indicated that all micron/nano COM and COD could damage the cell membrane; however, the membrane injury caused by micron-sized crystals was weaker than the nano-sized crystals.

#### **4.2 Nano-sized COM and COD produce toxicity by damaging cell membrane and mitochondria**

Nano-sized CaOx crystals (COM-50nm and COD-50nm) have two ways to interact with the cells, namely, adhering to the cell membrane and internalizing into the cells (Fig. 4). Both ways could cause cell injury, but the injury mechanism may be different (Fig. 9).

When the nano-sized crystals are internalized into the cells, they could disrupt the oxidant-antioxidant balance [22,23] and stimulate more ROS (Fig. 5). A direct relationship exist between the specific surface area of particles and ROS generation capability [24]. Small-sized crystals have larger specific surface area and more active sites than large-sized crystals under the same concentration; these active sites could capture oxygen molecules and produce superoxide radical through dismutation or Fenton reaction [23]. Excessive ROS could destroy intracellular large molecules, such as protein, lecithin, and nucleic acid, thereby hindering the information transmission line and the modulation of transcription factors [25,26]. Meanwhile, the internalized crystals could directly interact with mitochondria (Fig. 6) and cause a decrease in  $\Delta\psi_m$ , mitochondrial membrane permeability, and mitochondrial dysfunction [21,27]. Internalized crystals could also directly interact with the nucleus, and even enter the nucleus through the nuclear pores to injure the DNA, thereby causing cell cycle progression changes and cell arrest in the S phase (Fig. 7). A series of cell

responses would finally lead to cell death; nano-sized COM and COD mainly cause necrotic cell death (Fig.8), and a small number of cell apoptosis are also observed under high crystal concentration.

The crystal endocytosis process produces numerous intracellular signaling events to regulate cell function and status; crystal endocytosis also results in disruption of cell membrane and disorganization of cell cytoskeleton [28]; such membrane injury would cause necrotic cell death [29,30]. Internalized CaOx crystals of varying sizes and phases may increase the lysosomal membrane permeability in varying degrees. A prevalent assumption is that the reparable damage of lysosomes can initiate apoptosis and a sudden massive destruction of lysosomes leads to necrosis [31].

Micron/nano COM and COD could cause necrotic cell death in varying degrees and lead to a small number of cell apoptosis under high concentration. Borges et al. [32] demonstrated that the exposure of CaOx crystals induced necrotic cell death rather than apoptosis in proximal tubular cell line (LLC-PK1), whereas  $\text{Ox}^{2-}$  can cause Madin Darby-canine kidney cells apoptosis and necrosis. Schepers et al. [33] demonstrated that CaOx crystals (1–2  $\mu\text{m}$ ) exposure caused acute necrotic cell death rather than apoptosis in renal proximal tubule cells. However, Khan et al. [7] indicated that the exposure of cells to CaOx crystals resulted in significant apoptotic changes (condensation and margination of nuclear chromatin, DNA fragmentation) and certain necrotic changes (loss of plasma membrane integrity and release of lactate dehydrogenase). Thus, cell apoptosis and necrosis caused by CaOx may be related to crystal size, concentration, crystal phase, and cell types.

### 4.3 Differences in aggregation and damage capacity of COM and COD crystals

In the biological system, crystal size, zeta potential, and crystal phase play an important role in the crystal–cell interaction. With a transit time across the kidney of 5–10 min, the residence time is too short for crystals to nucleate and grow sufficiently large to be trapped. Some researchers have proposed that crystal aggregation is the most important step in stone formation [34,35]. In the

present study, the hydrodynamic size of COM-50nm (1342 nm) is 1.4 times larger than that of COD-50nm (953 nm), indicating that these nano-sized crystals are seriously aggregated and that COM-50nm aggregated more seriously than COD-50nm, whereas micron-sized COM and COD are more stable and are not aggregated as shown in SEM detection. The absolute value of zeta potential of COM-50nm in the culture medium is smaller than the COD-50nm; that is, COM-50nm is more unstable and could aggregate much easier. Therefore, nano-sized COM aggregates much easier to form bulk crystals and block the flow of urine from the kidney.

Furthermore, a significant difference in the interaction between COM, COD, and Vero exist because of the differences in their crystal structures. The  $\text{Ca}^{2+}$  surface site concentrations in the main ( $\bar{1}01$ ) face of COM (0.0542 sites/ $\text{A}^2$ ) is higher than the (100) face of COD (0.0439 sites/ $\text{A}^2$ ) [4]. Therefore, the adhesion force between the ( $\bar{1}01$ ) face of COM and expressed adhesion molecule (such as HA and OPN) on the surface of injured cells is higher than the (100) face of COD. Hence, COM adheres much easier on renal epithelial cells, and the following aggregation is more serious than in COD crystals, indicating that the numerous COMs present in urine have higher risk of forming kidney stones than COD.

## 5. Conclusions

Micron/nano COM and COD could decrease the cell viability and  $\Delta\psi_m$ ; increase LDH release, ROS level, and S phase arrest; and cause cell morphology change in Vero cells. Nano-sized crystals cause more serious cell injury than the micron-sized crystals, and their injury mechanisms are different. Micron-sized CaOx crystals mainly cause cell membrane injury, which leads to cell membrane dysfunction and even membrane fracture. Nano-sized COM and COD crystals could damage the membrane integrity by adhering crystals, as well as directly damage the mitochondria by internalized crystals, thereby leading to the dysfunction of mitochondria and cell death. The difference of toxicity between COM and COD of same size is associated with the crystal structure and surface charges. The study on the interaction mechanism between COM, COD, and renal

epithelial cells will provide a theoretical basis for clinical prevention and treatment of lithiasis

### Acknowledgements:

This work was supported by National Natural Science Foundation of China (NO. 21371077).

### Notes and references

- [1] Sun X Z, Shen L M, Cong X M, Zhu H Z, He L, Lu J L. Infrared spectroscopic analysis of 5,248 urinary stones from Chinese patients presenting with the first stone episode. *Urol. Res.*, 2011, 39: 339–343.
- [2] Farmanesh S, Ramamoorthy S, Chung J, Asplin J R, Karande P, Rimer J D. Specificity of growth inhibitors and their cooperative effects in calcium oxalate monohydrate crystallization. *J. Am. Chem. Soc.*, 2014, 136: 367–376.
- [3] Wesson J A, Ward M D. Pathological biomineralization of kidney stones. *Elements*, 2007, 3(6): 415–421.
- [4] Sheng X X, Ward M D, Wesson J A. Crystal surface adhesion explains the pathological activity of calcium oxalate hydrates in kidney stone formation. *J. Am. Soc. Nephrol.*, 2005, 16(7): 1904–1908.
- [5] Khand F D, Gordge M P, Robertson W G, Noronha–Dutra A A, Hothersall J S. Mitochondrial superoxide production during oxalate–mediated oxidative stress in renal epithelial cells. *Free. Radic. Biol. Med*, 2002, 32(12): 1339–1350.
- [6] Kohjimoto Y, Ebisuno M, Tamura T, Ohkawa T. Interactions between calcium oxalate monohydrate crystals and Madin–Darby canine kidney cells: endocytosis and cell proliferation. *Urol. Res.*, 1996, 24: 193–199.
- [7] Khan S R, Byer K J, Thamilselvan S, Hackett R L, McCormack W T, Benson N A, Vaughn K L, Erdos G W. Crystal–cell interaction and apoptosis in oxalate–associated injury of renal epithelial cells. *J. Am. Soc. Nephrol.*, 1999, 10 Suppl 14: S457–463.

- [8] Kanlaya R, Fong–Ngern K, Thongboonkerd V. Cellular adaptive response of distal renal tubular cells to high–oxalate environment highlights surface alpha–enolase as the enhancer of calcium oxalate monohydrate crystal adhesion. *J. Proteomics*, 2013, 80: 55–65.
- [9] McMartin K E, Wallace K B. Calcium oxalate monohydrate, a metabolite of ethylene glycol, is toxic for rat renal mitochondrial function. *Toxicol. Sci.*, 2005, 84: 195–200.
- [10] Meimaridou E, Jacobson J, Seddon A M, Noronha–Dutra A A, Robertson W G, Hothersall J S. Crystal and microparticle effects on MDCK cell superoxide production: oxalate–specific mitochondrial membrane potential changes. *Free Rad. Biol. Med.*, 2005, 38: 1553–1564.
- [11] Wang B–H, Wu B–H, Liu J, Yao W–M, Xia D, Li L, Chen Z–Q, Ye Z–Q, Yu X. Analysis of altered microRNA expression profiles in proximal renal tubular cells in response to calcium oxalate monohydrate crystal adhesion: implications for kidney stone disease. *PLoS One*, 2014, 7(9): 1–8.
- [12] Semangoen T, Sinchaikul S, Chen S–T, Thongboonkerd V. Altered proteins in MDCK renal tubular cells in response to calcium oxalate dihydrate crystal adhesion: a proteomics approach. *J. Proteome Res.*, 2008, 7(7): 2889–2896.
- [13] Yuen J W M, Gohel M–D I. The initial and subsequent inflammatory events during calcium oxalate lithiasis. *Clin. Chim. Acta*, 2010, 411: 1018–1026.
- [14] Sun X–Y, Ouyang J–M, Zhu W–Y, Li Y–B, Gan Q–Z. Size-dependent toxicity and interactions of calcium oxalate dihydrate crystals on Vero renal epithelial cells. *J. Mater. Chem. B*, 2015, 3(9): 1864–1878.
- [15] Sheng X X, Ward M D, Wesson J A. Adhesion between molecules and calcium oxalate crystals: Critical interactions in kidney stone formation. *J. Am. Chem. Soc.*, 2003, 125(10): 2854–2855.
- [16] Wang T, Thurgood L A, Grover P K, Ryall R L. A comparison of the binding of urinary calcium oxalate monohydrate and dihydrate crystals to human kidney cells in urine. *Bju Int.*, 2010,

106(11): 1768–1774.

- [17] Shapur N K, Uvarov V, Popov I, Katz R, Gofrit O N, Landau E H, Pode D, Duvdevani M. Crystallite size–Is it a new predictor for renal stone burden? *Urology*, 2012, 80(5): 980–985.
- [18] Duan C Y, Xia Z Y, Zhang G N, Gui B S, Xue J F, Ouyang J M. Changes in urinary nanocrystallites in calcium oxalate stone formers before and after potassium citrate intake. *Int. J. Nanomed.*, 2013, 8: 909–918.
- [19] Boya P. Lysosomal function and dysfunction: Mechanism and disease. *Antioxid. Redox Sign.* 2012, 17(5): 766-774.
- [20] Schepers M S J, Duim R A J, Asselman M, Romijn J C, Schroder F H, Verkoelen C F. Internalization of calcium oxalate crystals by renal tubular cells: A nephron segment–specific process? *Kidney Int.*, 2003, 64(2): 493–500.
- [21] Niimi K, Yasui T, Okada A, Hirose Y, Kubota Y, Umemoto Y, Kawai N, Tozawa K, Kohri K. Novel effect of the inhibitor of mitochondrial cyclophilin D activation, N–methyl–4–isoleucine cyclosporin, on renal calcium crystallization. *Int. J. Urol.*, 2014, 21(7): 707–713.
- [22] Akhtar M J, Ahamed M, Kumar S, Khan M A M, Ahmad J, Alrokayan S A. Zinc oxide nanoparticles selectively induce apoptosis in human cancer cells through reactive oxygen species. *Int. J. Nanomed.*, 2012, 7: 845–857.
- [23] Nel A, Xia T, Madler L, Li, N. Toxic Potential of Materials at the Nanolevel. *Science*, 2006, 311: 622–627.
- [24] Li Y, Sun L, Jin M, Du Z, Liu X, Guo C, Li Y, Huang P, Sun Z. Size–dependent cytotoxicity of amorphous silica nanoparticles in human hepatoma HepG2 cells. *Toxicol. In Vitro*, 2011, 25(7) 1343–1352.
- [25] Umekawa T. Editorial comment to renal tubular epithelial cell injury and oxidative stress induce calcium oxalate crystal formation in mouse kidney. *Int. J. Urol.*, 2010, 17(1): 92–93.

- [26] Jin C–Y, Zhu B–S, Wang X–F, Lu Q–H. Cytotoxicity of titanium dioxide nanoparticles in mouse fibroblast cells. *Chem. Res. Toxicol.*, 2008, 21(9): 1871–1877.
- [27] Hovda K E, Guo C G, Austin R, McMartin K E. Renal toxicity of ethylene glycol results from internalization of calcium oxalate crystals by proximal tubule cells. *Toxicol. Let.*, 2010, 192: 365–372.
- [28] Huang X L, Teng X, Chen D, Tang F Q, He J Q. The effect of the shape of mesoporous silica nanoparticles on cellular uptake and cell function. *Biomaterials*, 2010, 31: 438–448.
- [29] Liu Z, Xiao Y, Chen W, Wang Y, Wang B, Wang G, Xu X, Tang R. Calcium phosphate nanoparticles primarily induce cell necrosis through lysosomal rupture: the origination of material cytotoxicity. *J. Mater. Chem. B.*, 2014, 2(22): 3480–3489.
- [30] Thongboonkerd V, Semangoen T, Sinchaikul S, Chen S–T. Proteomic analysis of calcium oxalate monohydrate crystal–induced cytotoxicity in distal renal tubular cells. *J. Proteome Res.*, 2008, 7(11): 4689–4700.
- [31] Kroemer G, Jäätelä M. Lysosomes and autophagy in cell death control. *Nat. Rev. Cancer*, 2005, 5(11): 886–897.
- [32] Borges F T, Michelacci Y M, Aguiar J A K, Dalboni M A, Garofalo A S, Schor N. Characterization of glycosaminoglycans in tubular epithelial cells: Calcium oxalate and oxalate ions effects. *Kidney Int.*, 2005, 68(4): 1630–1642.
- [33] Schepers M S J, van Ballegooijen E S, Bangma C H, Verkoelen C F. Crystals cause acute necrotic cell death in renal proximal tubule cells, but not in collecting tubule cells. *Kidney Int.*, 2005, 68(4): 1543–1553.
- [34] Finlayson B, Reid F. The expectation of free and fixed particles in urinary stone disease. *Invest Urol.*, 1978, 15(6): 442–448.
- [35] Kok D J, Khan S R. Calcium oxalate nephrolithiasis, a free or fixed particle disease. *Kidney Int* 1994, 46(3): 847–854.

## Captions

Table 1. Physicochemical characterization of micron/nano COM and COD.

Fig. 1. SEM images (a–d), XRD spectra (e–h) and hydrodynamic size (i, j) of COM and COD crystals of varying sizes. (a, f, i) COM–50nm; (b, e) COM–10 $\mu$ m; (c, h, j) COD–50nm; (d, g) COD–10 $\mu$ m. Scale bars: (a) 200 nm; (c) 100 nm; (b, d) 5  $\mu$ m.

Fig. 2. Cytotoxicity of micron/nano COM and COD on Vero cells. The cell viability was detected by CCK–8 assay (a) and LDH release assay (b). Vero cells were incubated with different concentrations of micron/nano COM and COD for 6 h. Data were expressed as mean  $\pm$  SD from three independent experiments. Crystal concentration: 100  $\mu$ g/mL, 300  $\mu$ g/mL, 1000  $\mu$ g/mL

Fig. 3. Morphology detection of Vero cells and co–incubated crystals. SEM images of Vero cells after exposure to 300  $\mu$ g/mL micron/nano COM and COD crystals for 6 h. (a) COM–50nm; (b) COD–50nm; (c) COM–10 $\mu$ m; (d) COD–10 $\mu$ m.

Fig. 4. Confocal laser scanning microscopy (CLSM). Cell nuclei (blue) and cytoskeleton (green, as represented by F-actin) were stained with fluorescein isothiocyanate-conjugated (FITC) phalloidin and (4',6-diamidino-2-phenylindole) DAPI, respectively. COM crystals could be visualized by their ability to reflect the light at  $\lambda$  633 nm of Kr-laser (red). (A) Light reflection of plain COM crystals in red at  $\lambda$  633 nm. (B) Control cells without COM crystals. (C) COM-50nm was incubated with subconfluent Vero for 6 h; extracellular (adherent) and intracellular (internalized) crystals could be observed. (D) COM-10 $\mu$ m was incubated with subconfluent Vero for 6 h; only adherent crystals were observed. (Arrowhead: adherent crystals; Open arrow: internalized crystals).

Fig. 5. Detection of intracellular ROS level of Vero cells after exposure to 300  $\mu$ g/mL micron/nano COM and COD crystals for 6 h. (A) Histogram of intracellular ROS level; (B) quantitative fluorescence intensity of intracellular ROS level. Data were expressed as mean  $\pm$  SD from three independent experiments.

Fig. 6. The effects of different concentrations of micron/nano COM and COD exposure on mitochondrial membrane potential ( $\Delta\psi_m$ ) in Vero cells. (A) Dot plots of  $\Delta\psi_m$  after incubation with COD-50nm and COD-10 $\mu$ m; (B) dot plots of  $\Delta\psi_m$  after incubation with COM-50nm and COM-10 $\mu$ m for 6 h; (C) quantitative histogram of  $\Delta\psi_m$ . Data were expressed as mean  $\pm$  SD from three independent experiments.

Fig. 7. The effects of exposure to micron/nano COM and COD crystals on cell cycle of Vero cells. (A) Representative images of cell cycle of Vero cells after exposure to COD-50nm, COD-10 $\mu$ m, COM-50nm and COM-10 $\mu$ m with the concentration of 300  $\mu$ g/mL for 6 h. (B) Quantitative histogram of cell cycle. Data were expressed as mean  $\pm$  SD from three independent experiments.

Fig. 8. Flow cytometric data of cell death after Vero cells were exposed to different concentrations of micron/nano COM and COD crystals for 6 h. The representative dot plots (A) and quantitative histogram results (C) of cellular apoptosis and necrosis after exposure to COD-50nm and COD-10 $\mu$ m. The representative dot plots (B) and quantitative histogram results (D) of cellular apoptosis and necrosis after exposure to COM-50nm and COM-10 $\mu$ m. Quadrants Q1, Q2, Q3, and Q4 denote the ratio of necrotic cells, necrotic and/or late apoptotic cells, normal cells, and early apoptotic cells, respectively.

Fig. 9. Suggested schematic illustration of cellular mechanism of Vero cell injury after exposure to micron/nano COM and COD crystals. COD-10 $\mu$ m and COM-10 $\mu$ m was only adhered on cell surface or partly internalized, leading to cell membrane dysfunction and even membrane fracture. COD-50nm and COM-50nm not only could damage membrane integrity by adhered crystals but also directly damage mitochondria by internalized crystals, thus leading to cell death.

Table 1. Physicochemical characterization of micron/nano COM and COD

	Size using SEM	Hydrodynamic size in DMEM / nm	PDI	specific surface $S_{BET}$ / m <sup>2</sup> /g	Zeta potential in DMEM / mV
COM-50nm	47.7 ± 6.2 nm	1342 ± 131	0.23 ± 0.08	26.3	2.1 ± 0.4
COM-10μm	9.67 ± 1.76 μm	—	—	0.83	-8.2 ± 1.8
COD-50nm	44.1 ± 8.7 nm	953 ± 98	0.28 ± 0.05	40.8	6.3 ± 0.9
COD-10μm	9.58 ± 0.97 μm	—	—	0.31	-12.0 ± 1.2

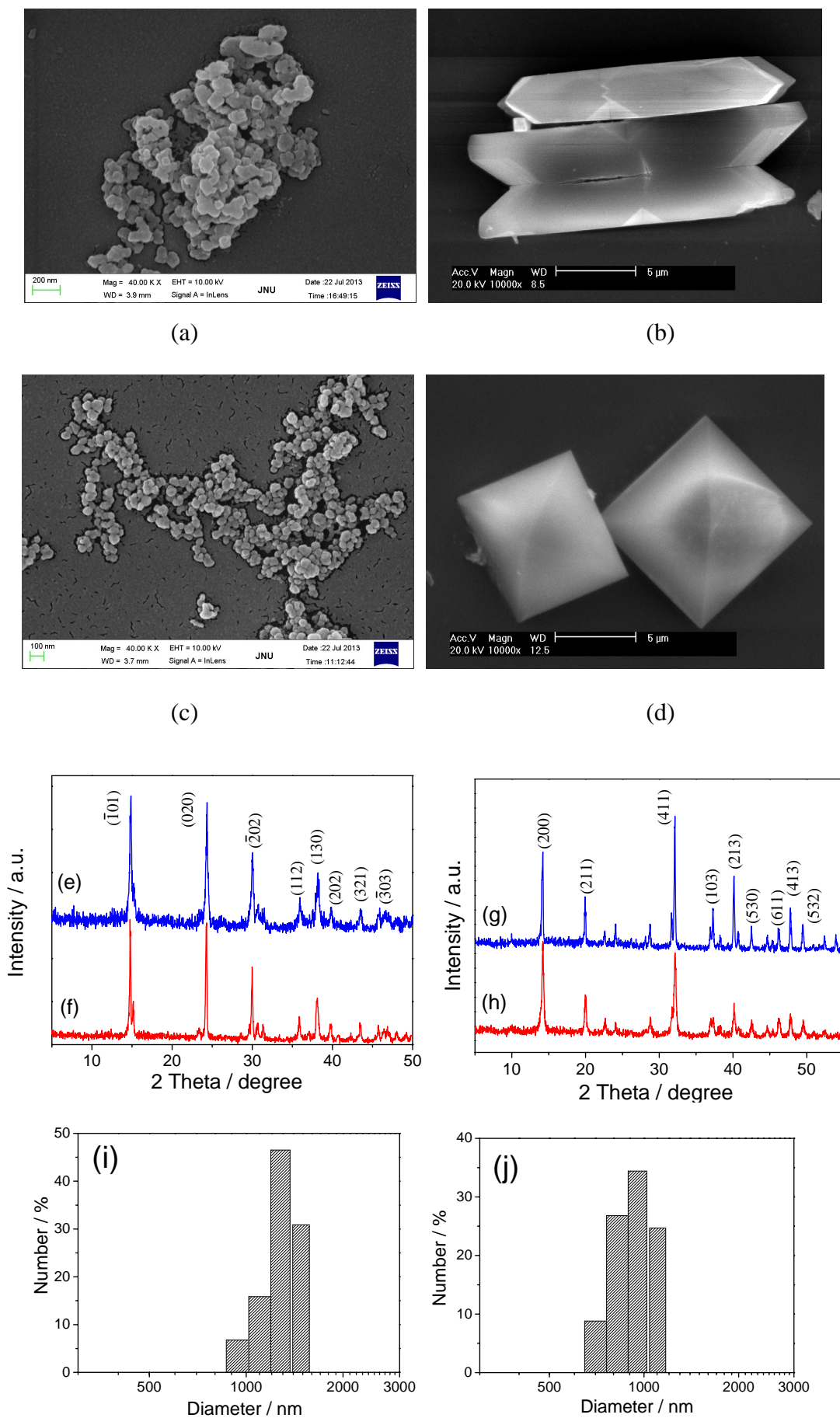


Fig. 1.

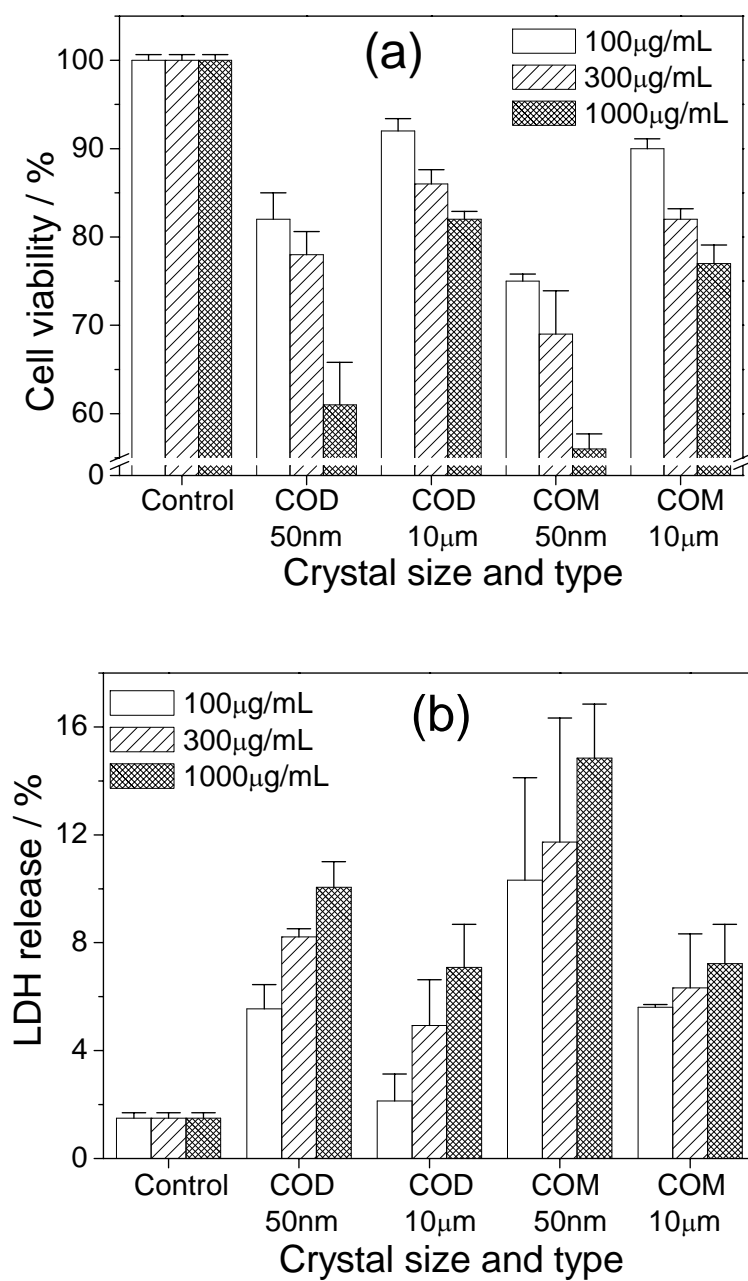


Fig. 2.

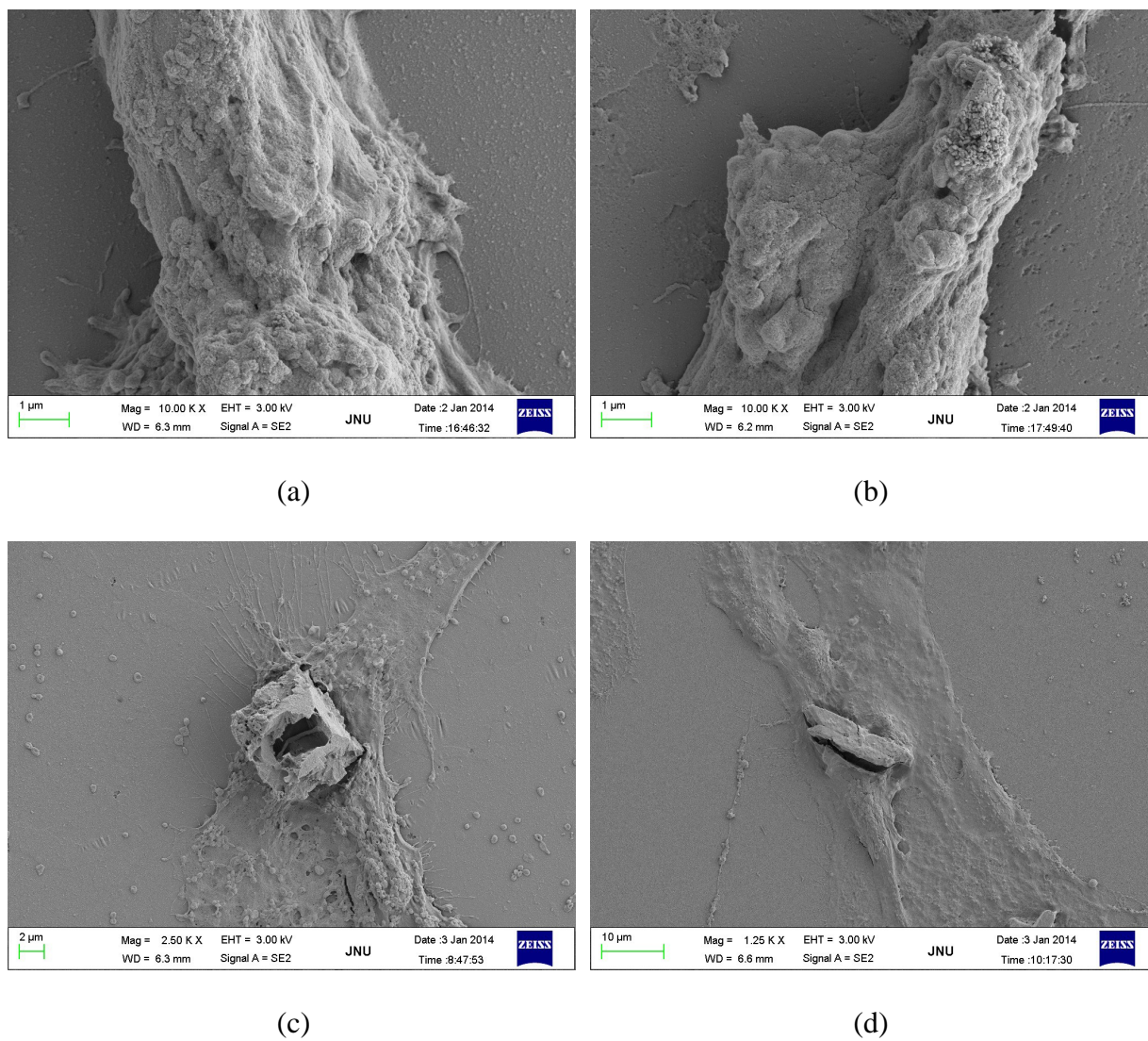
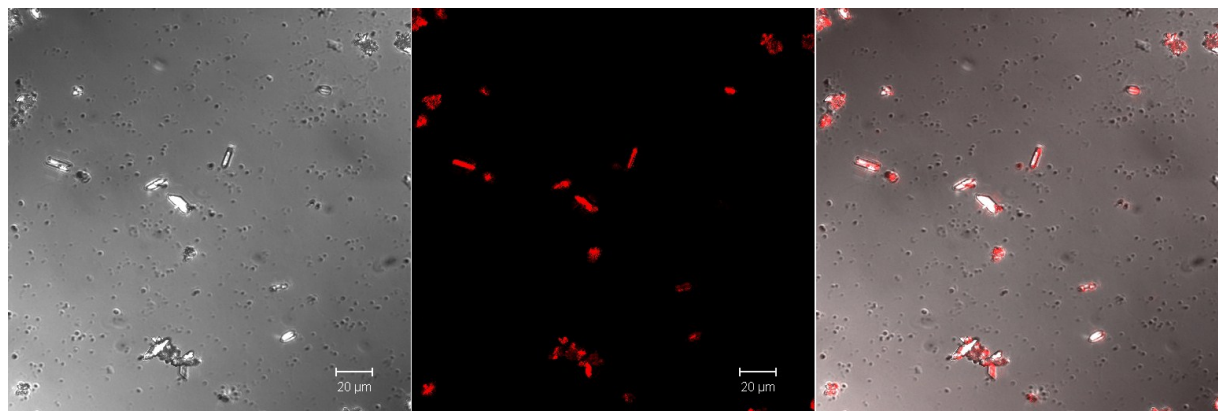
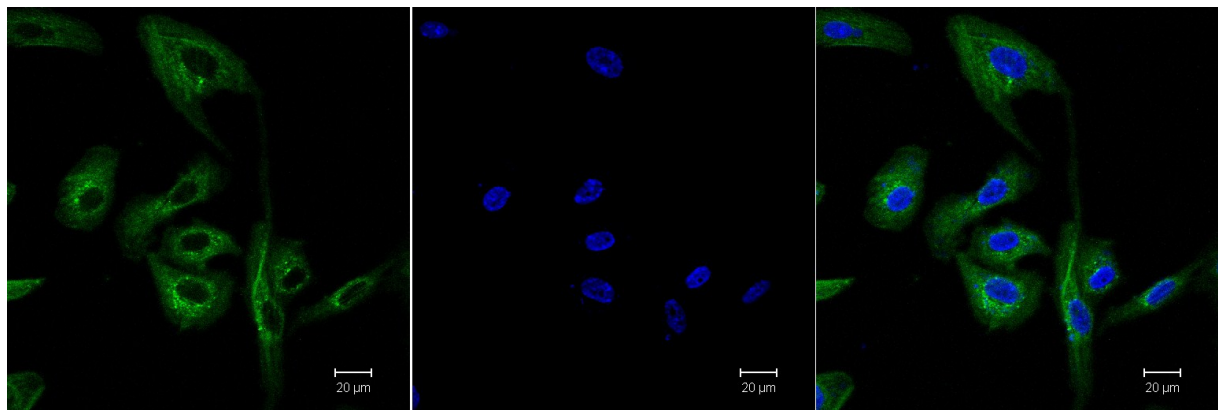


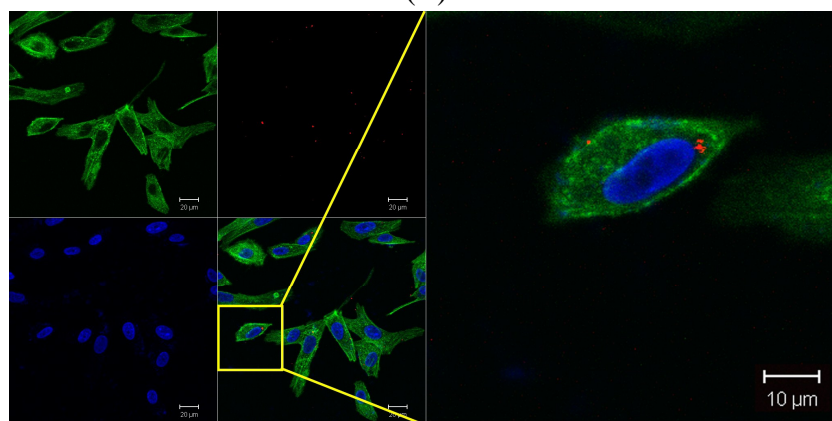
Fig. 3.



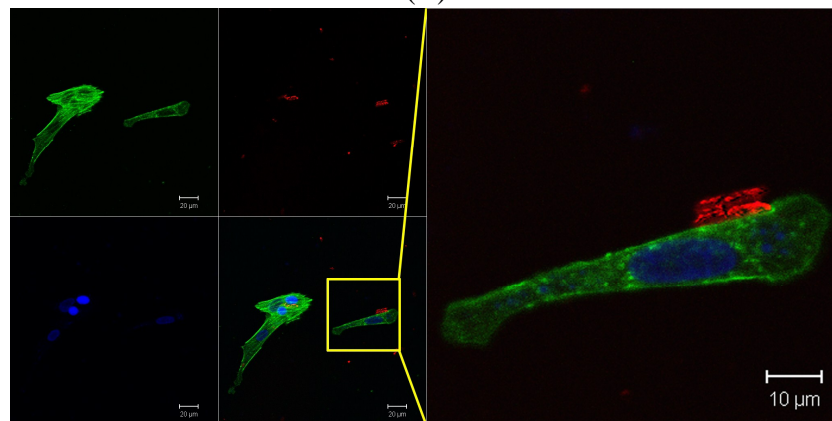
(A)



(B)



(C)



(D)

Fig. 4.

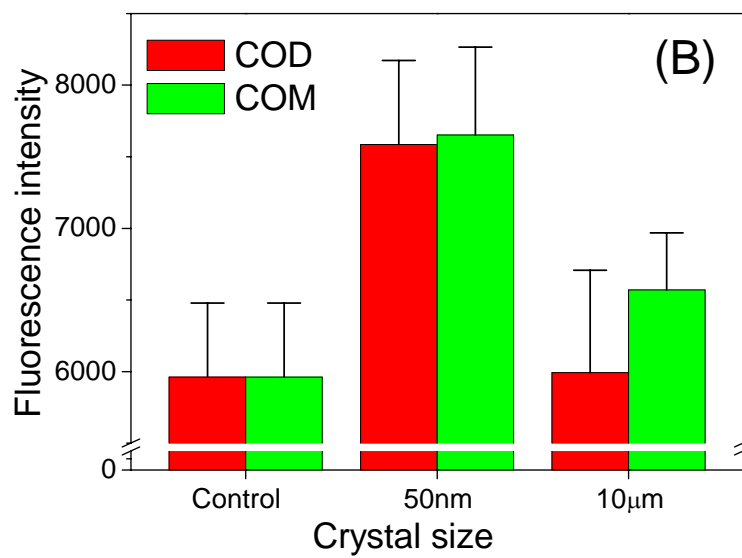
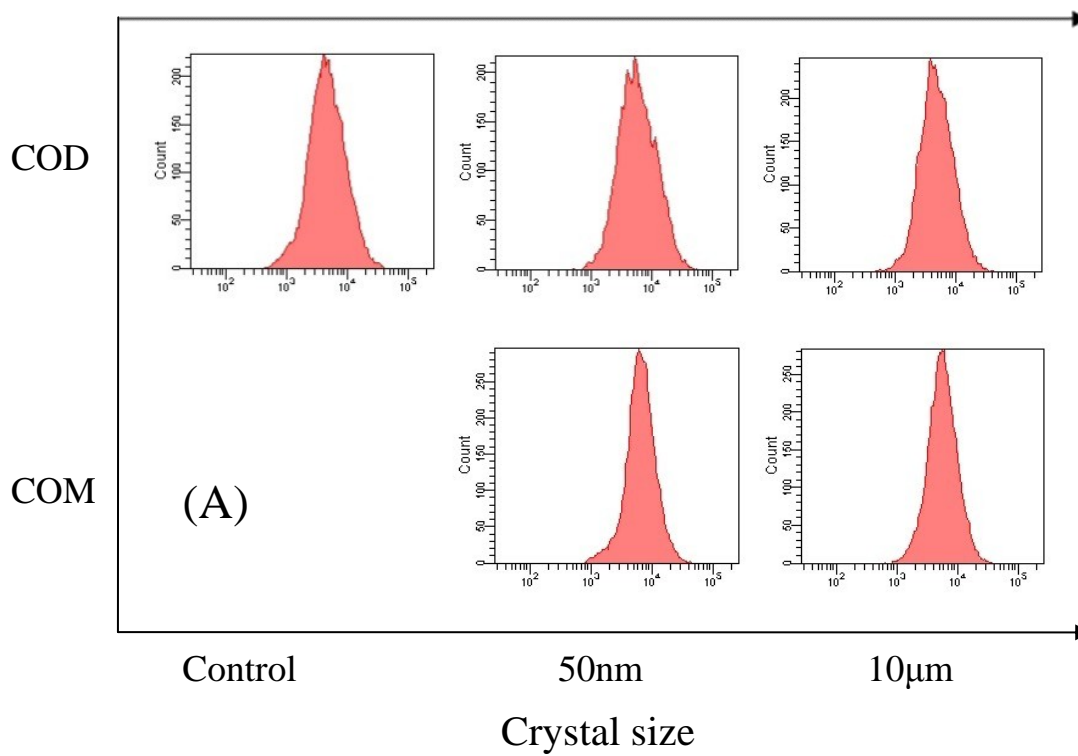


Fig. 5.

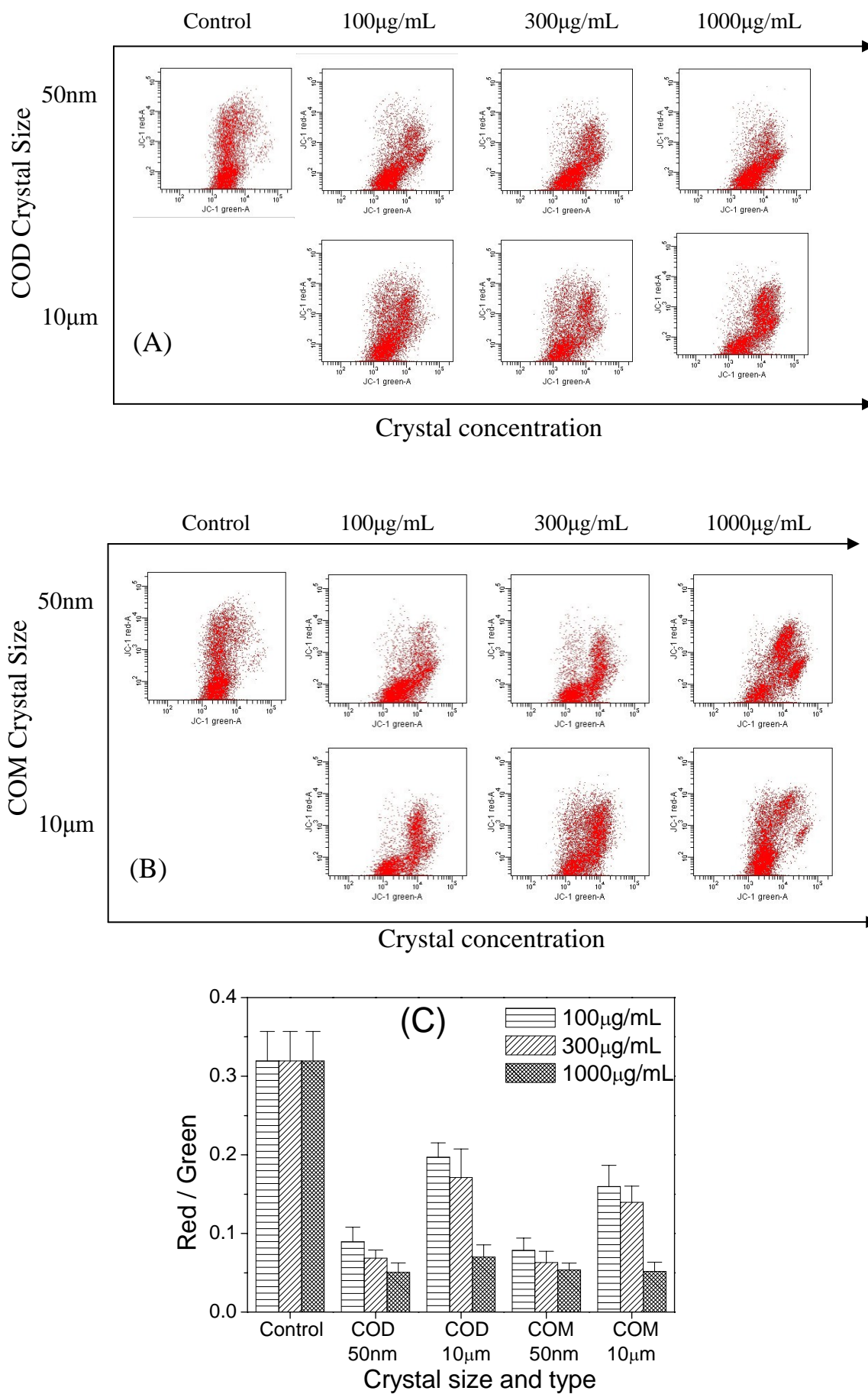


Fig. 6.

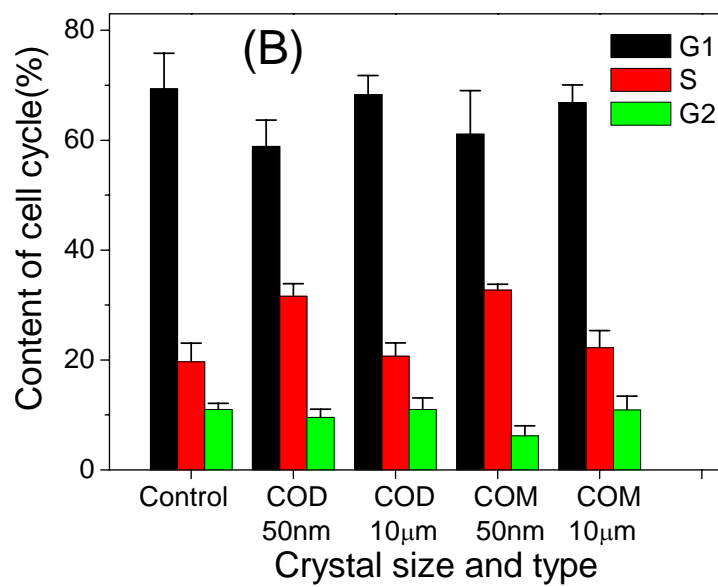
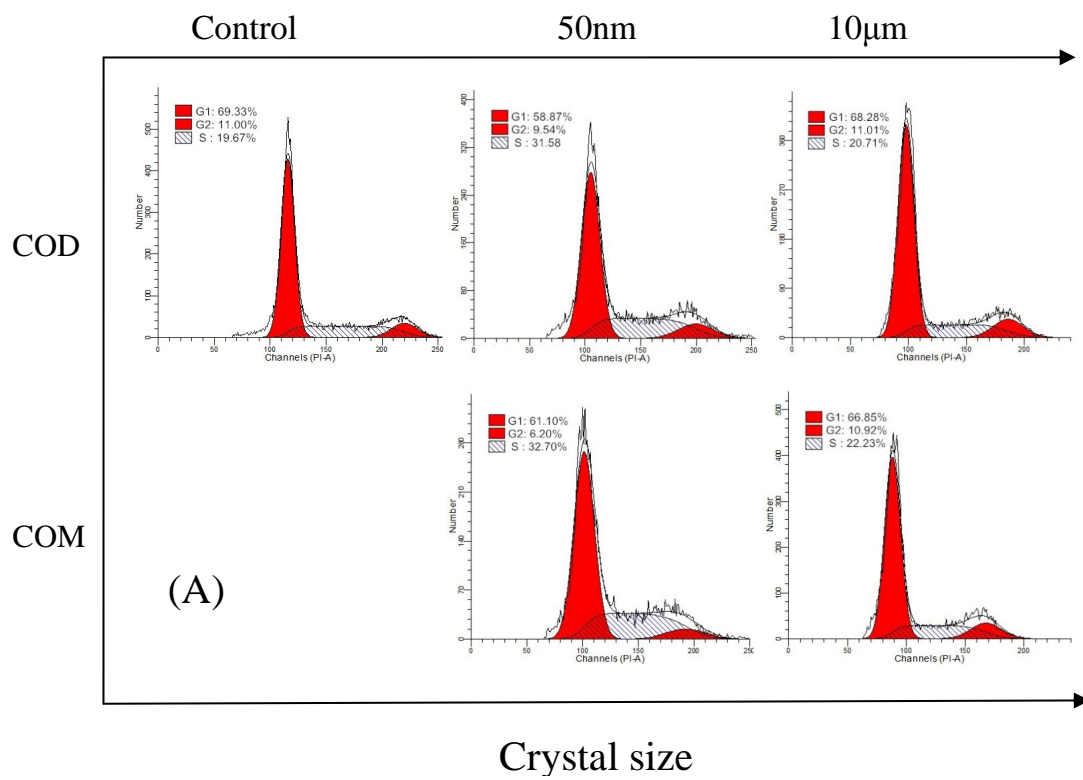


Fig. 7.

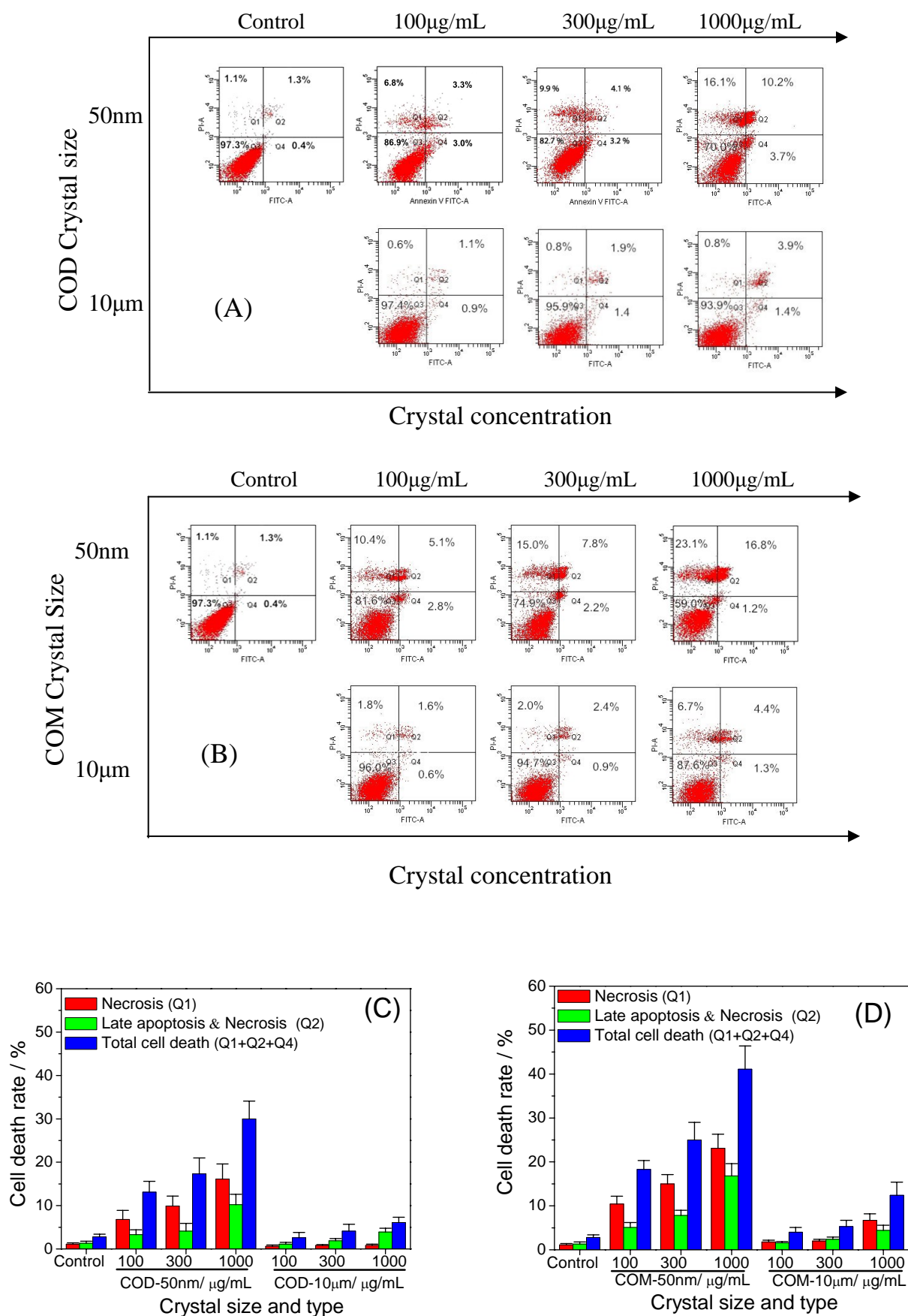


Fig. 8.

RSC Advances Accepted Manuscript

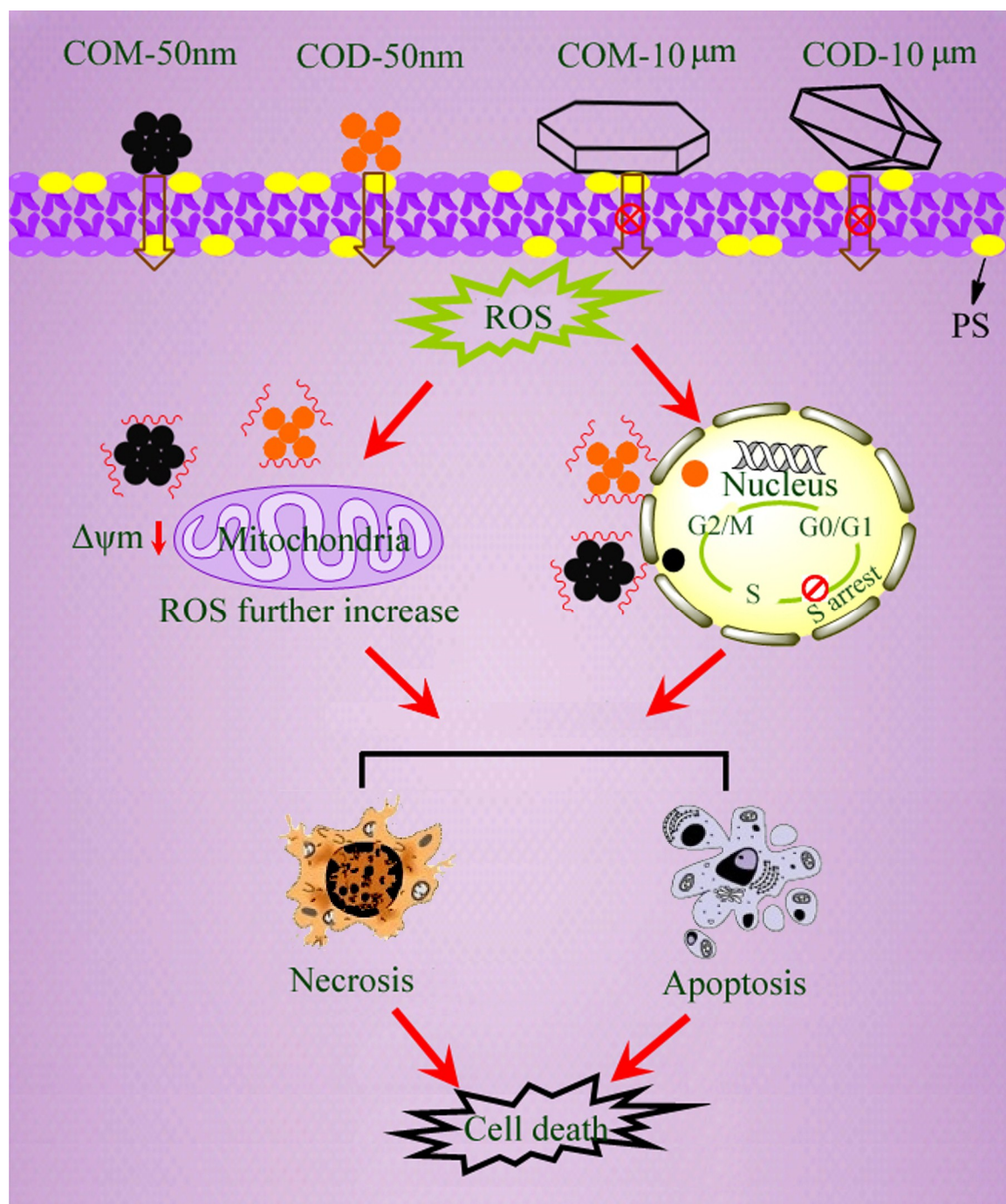


Fig. 9.